ISSN 0915-633X

NATIONAL INSTITUTE FOR FUSION SCIENCE

Plasma Parameter Estimations for the Large Helical Device Based on the Gyro-Reduced Bohm Scaling

M. Okamoto, N. Nakajima and H. Sugama

(Received – Sep. 17, 1991)

NIFS-114 Oct. 1991

RESEARCH REPORT
NIFS Series

This report was prepared as a preprint of work performed as a collaboration research of the National Institute for Fusion Science (NIFS) of Japan. This document is intended for information only and for future publication in a journal after some rearrangements of its contents.

Inquiries about copyright and reproduction should be addressed to the Research Information Center, National Institute for Fusion Science, Nagoya 464-01, Japan.

NAGOYA, JAPAN

Plasma Parameter Estimations for the Large Helical Device Based on the Gyro-Reduced Bohm Scaling

Masao OKAMOTO, Noriyoshi NAKAJIMA, and Hideo SUGAMA

National Institute for Fusion Science

Chikusa, Nagoya 464-01

Abstract

A model of gyro-reduced Bohm scaling law is incorporated into a one-dimensional transport code to predict plasma parameters for the Large Helical Device (LHD). The transport code calculations reproduce well the LHD empirical scaling law and basic parameters and profiles of the LHD plasma are calculated. The amounts of toroidal currents (bootstrap current and beam-driven current) are also estimated.

Keywords : Large Helical Device, transport code, gyro-reduced Bohm scaling, LHD scaling, bootstrap current, beam driven current

1. Introduction

Sudo et al.[1] obtained an empirical scaling law for the energy confinement time and the critical density limit from the analyses of experimental data of Heliotron E, W7–A, Heliotron DR and L2 stellarator. This scaling law holds for a wide range of plasma parameters of these stellarators and torsatrons and is called the LHD scaling law. Murakami et al.[2] reported that the global energy confinement times obtained in the ATF experiments can be well scaled by the gyro-reduced Bohm (GRB) scaling law based on the collisionless drift wave turbulence. Recent CHS experimental data [3] agree approximately with the GRB scaling law. Sudo[4] compared the LHD empirical scaling with the GRB scaling law and concluded that the GRB scaling law predicts practically the same parameters as the LHD scaling law. It was also reported [5] that the regression coefficients of the W7–AS empirical scaling law are very similar to those of LHD or GRB scaling law although the W7–AS scaling law has a weak dependence on the edge rotational transform and the minor radius dependence is not so strong ($\tau_E^{W7AS} \propto a^{1.28\pm0.16}$).

In this report we predict plasma parameters of the Large Helical Device using the LHD or GRB scaling law. A model transport coefficient based on the GRB scaling law is incorporated into a one-dimensional transport code to predict the plasma parameters and their profiles for the proposed LHD machine parameters. The obtained plasma profiles are used to calculate the bootstrap current and beam driven current.

2. LHD scaling

The LHD empirical scaling law for the energy confinement time τ_E and the critical density n_c are given by [1]

$$\tau_E[\mathrm{s}] = 0.17 P^{-0.58} n^{0.69} B^{0.84} a^{2.0} R^{0.75} \tag{2.1}$$

$$n_c[10^{20}\mathrm{m}^{-3}] = 0.25 P^{0.5} B^{0.5} a^{-1.0} R^{-0.5} \tag{2.2}$$

where P[MW] is the absorbed power, $n[10^{20}\mathrm{m}^{-3}]$ the line averaged density, B[T] the magnetic field, a[m] the minor radius and R[m] the major radius. Equation (2.1) is called the "LHD scaling law". The energy confinement time τ_E and the plasma beta value β are defined by $\tau_E = \frac{3}{2}(n_e T_e + n_i T_i) V_p / P$ and $\beta = 2\mu_0 (n_e T_e + n_i T_i)/B^2$, respectively, where n_e and n_i are the electron and ion densities, T_e and T_i the electron and ion temperatures, and V_p the plasma volume. Assuming $n_e = n_i = n$, $T_e = T_i = T$ and using the plasma volume $V_p = 2\pi^2 R a^2$, eq.(2.1) gives [1]

$$T[\mathrm{keV}] = 0.18 P^{0.42} n^{-0.31} B^{0.84} R^{-0.25} \tag{2.3}$$

$$\beta[\%] = 1.44 P^{0.42} n^{0.69} B^{-1.16} R^{-0.25}. \tag{2.4}$$

Substituting eq.(2.2) into eq.(2.4) yields the LHD scaling critical beta value. We apply eqs.(2.1)–(2.4) to the Large Helical Device (LHD). However we should note that the configuration effects such as rotational transform ι, helical ripple strength ϵ_h or magnetic axis shift Δ_{axis} are not seen in the LHD scaling although plasma stored energy increases with the inward plasma shift in NBI experiments of CHS [3]. Another problem in the LHD scaling is the uncertain estimation of heating input power(power deposition) from the neutral beam injection. Therefore it is noted that the LHD scaling based on the experimental data of existing devices has some errors and the plasma parameters predicted by the extrapolation to the larger device (LHD) may have large errors.

The proposed basic parameters for the LHD are $L = 2$, $M = 10$, $R = 3.9$ m, $B = 4$ T, $\gamma_c = 1.25$ and $\alpha = 0.1$, where L and M are poloidal and toroidal polarities, γ_c the pitch parameter of winding law, and α the pitch modulation parameter [6]. To obtain a good single particle confinement compatible with a high plasma beta value, we require the inward plasma shift of $\Delta_{axis} \simeq -0.15m$ and $B_Q(net) \simeq 0$, where Δ_{axis} is the magnetic

axis shift of the vacuum field, and $B_Q(net)$ is the net quadrupule field created by helical and poloidal coils [6–8]. In this case the toroidally averaged plasma cross section is nearly circular and the average minor radius of the outermost closed surface in the vacuum field is roughly 0.6 ~ 0.65 m. We refer these machine parameters to the standard configuration below.

Figure 1 shows the dependence of the energy confinement time τ_E, the temperature T and the beta value β on the input power P and the density n. Here the critical density n_c is also shown and we have used $R = 3.9$ m, $B = 4$ T and $a = 0.65$ m in Fig 1. The LHD scaling depends strongly on the plasma radius, but it is generally difficult to determine the definite plasma radius in helical systems since magnetic islands are easily created in the peripheral region due to field errors and finite beta effects. Therefore it should be noted that the employed minor radius ($a = 0.65m$) deduced from calculated vacuum magnetic fields is the most optimistic one.

From Fig.1 we can see, for example, that $\tau_E = 112$ ms, $T = 1.44$ keV and $\beta = 0.72$ % for $P = 20$ MW and $n = 1 \times 10^{20}$ m^{-3}. For the same input power, we can obtain the critical density $n_c \simeq 1.7 \times 10^{20}$ m^{-3} at which $\tau_E = 165$ ms and $T = 1.22$ keV and $\beta = 1.1$ %. If the plasma minor radius is reduced to 0.6 m, we obtain $\tau_E = 96$ ms, $T = 1.44$ keV and $\beta = 0.72$ % for $n = 1 \times 10^{20}$ m^{-3} and $P = 20$ MW.

3. Transport code study

Here we use a one-dimensional transport code in order to obtain the plasma profiles reproducing the LHD empirical scaling law. Goldston et al.[9] derived a scaling similar to the LHD scaling by the mixing length argument of the collisionless drift wave turbulence as follows. Assuming that the spatial variation of the density fluctuation $k_\perp \tilde{n}$ is not larger than that of background density n/L_n in the quasilinear theory of collisionless drift waves, we have the turbulent diffusivity $\chi_e \simeq \gamma/k_\perp^2$[10]. Here putting $\gamma \simeq \omega_{*e} = (T/eB)(k_\perp/L_n)$, $k_\perp \simeq \rho_s = \sqrt{T_e/m_i\Omega_i^2}$, and $L_n \simeq a$ yields

$$\chi_e = \frac{T_e}{eB}\frac{\rho_s}{a} \tag{3.1}$$

which is called the "Gyro-Reduced Bohm" (GRB) scaling since it has the form of the Bohm diffusivity multiplied by ρ_s/a. Using $\tau_E = a^2\kappa/4\chi_e = \frac{3}{2}(n_eT_e + n_iT_i)V_p/P$ and $V_p = 2\pi^2 Ra^2\kappa$ with κ the elongation, we obtain

$$\tau_E^{dw} = 0.25P^{-0.6}n^{0.6}B^{0.8}R^{0.6}a^{2.4}\kappa A_i^{-0.2} \tag{3.2}$$

where A_i is the mass ratio of the plasma ion to the proton. Murakami et al.[2] reported that the experimental data of ATF are consistent with the GRB scaling (3.2). Sudo[4] compared the LHD empirical scaling (2.1) with the GRB scaling (3.2) and concluded that the GRB scaling predicts practically the same plasma parameters as those of the LHD empirical scaling. It should be noted that eq.(3.1) gives the dependence of χ_e on the temperature and the magnetic field as $\chi_e \propto T^{1.5}/B^2$, which is in good agreement with the experimental result obtained by Sano et al.[11] that in the NBI experiments of Heliotron E the electron thermal diffusivity have the dependence $\chi_e^{HE} \propto T_e^{1.52}B^{-2.0}$ at $r/a \sim 2/3$ (its absolute values are $\chi_e^{HE}(r = 2a/3) = 1 \sim 10$ m^2/s). However according to the GRB scaling (3.1) χ_e is decreased with increasing the radial coordinate while generally in the experiments χ_e is large in the peripheral region [12]. Thus although eq.(3.1) is possible to determine the global energy confinement time it does not seem to be valid locally.

Hagan and Frieman [13] applied the scale invariance technique [14] to the nonlinear gyro-kinetic equation [15] which describes low frequency ($\omega \leq \omega_{ci}$) microscopic ($k_\perp \sim \rho_i^{-1}$) fluctuations such as those of drift wave turbulence. They derived the thermal diffusivity due to electrostatic fluctuations, which has the form [13,16]

$$\chi = \frac{T_i}{eB}\frac{\rho_i}{a}F\left(\frac{\nu a}{v_{th}}, \beta, \iota, \epsilon, \kappa, \frac{L_j}{L_k}, \cdots\right) \tag{3.3}$$

where ρ_i is the ion Lamor radius, v_{th} the thermal velocity, ν the collision frequency, β the local plasma beta, ι the local rotaional transform, κ the flux surface elongation and L_j and L_k denote additional local scale lengths such as shear length $L_s = |\nabla\iota/\iota|^{-1}$, density length $L_n = |\nabla n/n|^{-1}$ and temperature length $L_T = |\nabla T/T|^{-1}$. When $T_e = T_i$, eq.(3.3) leads to GRB scaling (3.1) except for the arbitrary function F, which cannot be determined by the scale invariance technique alone. There may be a possibility that the thermal diffusivity given by eq.(3.3) increases at the plasma edge, which the GRB scaling (3.1) fails to predict, through L_n and other variables in the arbitrary function F.

Here we employ the GRB scaling for the electron thermal diffusivity in the simulations but we assume that $\chi_e(r)$ has the large values in the peripheral region through the function F in eq.(3.3). We use the transport code developed by Nakamura and Wakatani [17,18]. In the simulations the particle flux Γ is the sum of the neoclassical part Γ^{NC} and the anomalous part Γ^{AN}. In the same way the electron thermal flux Q_e consists of Q_e^{NC} and Q_e^{AN}. However we assume that the ion thermal flux Q_i contains Q_i^{NC} alone. In the neoclassical transport we consider both the axisymmetric part and the non-axisymmetric part (ripple transport). We use the expression for the ripple transport based on the single-helicity model magnetic field, which is derived by Hasting et al.[19] The anomalous transport Γ^{AN} and Q_e^{AN} are assumed to be proportional to only the gradients of density and electron temperature, respectively. The density diffusion coefficient D^{AN} and the electron thermal diffusivity χ_e^{AN} are given by

$$D^{AN} = \left(\frac{1}{3} \sim \frac{1}{5}\right) \chi_e^{AN} \tag{3.4}$$

$$\chi_e^{AN} = \langle \chi_e^{dw} \rangle (1 + f(r/a)^g)(g+2)/(g+2+2f) \tag{3.5}$$

$$\langle \chi_e^{dw} \rangle = \frac{\langle T_e \rangle}{eB} \frac{\langle \rho_s \rangle}{a} \tag{3.6}$$

where $\langle \cdot \rangle$ denotes the volume average. If we take the volume average of eq.(3.5), we have the GRB diffusivity in eq.(3.6). Here f and g are the parameters which determine the radial profile of χ_e^{AN}. We use $f = 4 \sim 6$ and $g = 5 \sim 10$, which give $\chi_e^{AN}(r)$ having the larger values near the plasma surface. The transport code used here enables the plasma to reach a given value of the volume average density $\langle n_e \rangle$ or the line average density $\bar{n}_e$ by the feedback control of gas puffing. We consider the electron cyclotron wave heating (ECW heating) and neutral beam injection heating (NBI heating). For simplicity the absorption profile for the ECW heating is fixed : $P_{ECW} \propto (1 - (r/a)^p)^q$. In the case of NBI heating the birth profile of the fast ions by the NBI is calculated and the Fokker-Planck equations are solved on each magnetic surface for fast ions to obtain the heat input to electrons and plasma ions. We use the vacuum magnetic field data for the rotaional transform $\iota(r)$ and the helical ripple field strength $\epsilon_h(r)$. In a wide range of parameters; $R_0 = 3.5 \sim 4$ m, $a = 0.52 \sim 0.65$ m, $B = 3 \sim 4$ T, $\bar{n}_e = (0.5 \sim 2.0) \times 10^{20}$ m^{-3} and $P = 5 \sim 20$ MW, the tranport code calculations reproduce the LHD scaling very well when $f \simeq 5$ and $g \simeq 8$. The results are shown in Fig.2(a) and (b), where calculated volume averaged temperature

$(\langle T_e\rangle + \langle T_i\rangle)/2$ and global energy confinement time τ_E^{Cal} are plotted versus those of the LHD scaling.

Figure 3 shows a result from the transport code calculations for the standard configuration. We have employed the outermost surface with the average radias of 0.62 m ($a = 0.62$ m). We have used $\epsilon_h(r)$ given by the vacuum magnetic field calculation with parameters described in §2 (for instance, $\epsilon_h(a) = 0.288$ and $\epsilon_h(a/2) = 0.05$). We assumed that $Z_{eff} = 2.0$, $D^{AN} = \chi_e^{AN}/3$, $f = 5$ and $g = 8$. In the case of Fig.3 we considered only the ECW heating with a parabolic heat deposition profile ($p = 2$, $q = 1$), and $P_{ECW} = 20$ MW. By the feedback control the density has been kept constant to be $\langle n_e\rangle = 1 \times 10^{20} m^{-3}$. Figure 3(a) shows the density profile. The profile is flattened in the inner region and has the peak in the outer region since the recycling of particles is localized outside and the mechanism of the inward particle diffusion is not included. Accordingly the line average density $\bar{n}_e$ is close to the volume average density $\langle n_e\rangle$; $\langle n_e\rangle \simeq \bar{n}_e \simeq 1 \times 10^{20}$ m^{-3}. Figure 3(b) shows the temperature profiles. The solid curve represents the electron temperature $T_e(r)$ and the broken curve the ion temperature $T_i(r)$. We obtain $T_e(0) = 4.05$ keV, $\langle T_e\rangle = 1.59$ keV, $T_i(0) = 2.78$ keV and $\langle T_i\rangle = 1.29$ keV, so that $T_e(0)/\langle T_e\rangle = 2.5$ and $T_i(0)/\langle T_i\rangle = 2.1$ implying that the ion temperature profile is very close to parabolic one and the electron profile is slightly steeper than that. Figure 3(c) and (d) show the electron thermal diffusivity $\chi_e(r)$ and the ion thermal diffusivity $\chi_i(r)$, respectively. The axisymmetric and nonaxisymmetric neoclassical transports and the anomalous transport are shown separately. (The ion anomalous transport χ_i^{AN} is not included in the calculation.) The total thermal diffusivities $\chi_e(r)$ and $\chi_i(r)$ are shown by the solid curves. For electrons, the ripple diffusion has a maximum value at $r \simeq a/2$ ($\chi_e^{NC} \simeq 0.45$ m^2/s) but χ_e is almost determined by χ_e^{AN} in the whole region. The total electron thermal diffusivity χ_e changes from $0.5 \sim 4$ m^2/s. For ions, χ_i is determined by the ripple diffusion which has very large values at $r \simeq a/2$ ($\chi_i = \chi_i^{NC} \simeq 4.0 \sim 5.0$ m^2/s) but is very small in the peripheral region. The global energy confinement time, which is defined as the internal energy devided by the input power, $\tau_E^G = (W_e + W_i)/P$, is 97 ms. The LHD empirical scaling equations (2.1) and (2.3) give $\tau_E^{LHD} = 102$ ms and $T^{LHD} = 1.44$ keV, which are consistent with our simulation results $\tau_E^G = 97$ ms and $\langle T\rangle = (\langle T_e\rangle + \langle T_i\rangle)/2 = 1.44$ keV. The calculation shows that the electron

anomalous heat flux across the outermost surface $4\pi^2 Raq_e^{AN}(a)$ exceeds the neoclassical electron heat flux and anomalous and neoclassical ion heat fluxes. Therefore the electron anomalous heat balance has the dominant effect on the total energy confinement time. The magnitude of χ_e in the peripheral region is very sensitive to the global confinement time. The total confinement time defined as the internal plasma stored energy devided by the heat flux across the outermost surface, $\tau_E^T = -(W_e + W_i)/4\pi^2 Ra(q_e(a) + q_i(a))$, is 120 ms. Figure 3(e) shows the collision parameters $\nu_{e**} = \nu_e/(\epsilon_h \omega_h)$ and $\nu_{i**} = \nu_i/(\epsilon_h \omega_h)$ where $\omega_h = \epsilon_h^{3/2}\omega_p$ and $\omega_p = v_{th}/qR$. We see that both electrons and ions are in the $1/\nu$ regime in the region 0.15 m $< r <$ 0.55 m. Figure 3(f) shows the electrostatic potential $\Phi(r)$. The radial electric field E_r are calculated by the condition $\Gamma_e = \Gamma_i$. Putting $\Phi = 0$ at $r = a$, $\Phi(r)$ are obtained from E_r. We have $e\Phi/T_e \simeq 2.0$ and $e\Phi/T_i \simeq 2.6$ at $r/a \simeq 0.5$.

Here we used the single-helicity model magnetic field in order to calculate the ripple diffusion. However the actual magnetic field configuration has the mulptiple-helicity for which the ripple diffusion is different from that for the single-helicity. Todoroki[8] and Nakajima et al.[20] studied the dependence of the ripple diffusion on the magnetic field configuration (effects of the magnetic axis shift, the helical coil pitch modulation, the flux surface elongation etc.) in the $1/\nu$ regime and found that the ripple diffusion is remarkably decreased by the inward shift of the plasma in terms of the vertical magnetic field. Ogawa et al. calculated ripple diffusions in detail for the LHD plasma by the DKES code [21] and obtained $\chi_e^{DKES} \simeq 0.2$ m^2/s and $\chi_i^{DKES} \simeq 2$ m^2/s at $r/a \simeq 0.5$ for parameters of $n_e \simeq 10^{20}$ m^{-3}, $T_e \simeq 2.0$ keV, $T_i \simeq 2.0$ keV and $e\Phi/T_i \simeq 2 \sim 3$ when the magnetic axis is shifted inward by 0.2 m and $B_Q(net) \simeq 0$. The values of thermal diffusivities with single-helicity model, χ_e^{NC} and χ_i^{NC}, calculated in the present transport code are overestimated by a factor of 2. However as described above the electron anomalous transport dominates over the neoclassical transports this descrepancy is not important. Thus the simulation results of our transport code indicate that not the ripple diffusion but the anomalous transport χ_e^{AN} in the plasma edge has the dominant effect on the global plasma confinement for the plasma with the 15 cm inward shifted magnetic axis. Here the anomalous transport is considered only for the electron but actually it is supposed that the anomalous ion transport exists and χ_i^{AN} in the plasma edge also has the significant effect on the confinement.

Figure 4 shows the result in the case of NBI heating. Two hydrogen neutral beams with energy of 125 keV are tangentially injected from the negative ion sources in the co and counter directions, respectively. The shape of the beam cross section is assumed to be Gaussian with a halfwidth of 0.15 m. The distance from the toroidal center to the beam line is chosen 3.7 m. The birth points of fast ions are first calculated and subsequently the Fokker-Planck equations are solved for the fast ion slowing down process to obtain the heat input to electrons and plasma ions. The port through power of NBI is 20 MW and a small amount of ECW power ($P_{ECW} = 3$ MW) is added. Other calculation parameters are the same as in Fig.3 At the steady state absorbed powers by electrons and ions from NBI are $P^e_{NBI} = 11.31$ MW and $P^i_{NBI} = 6.10$ MW, respectively. (The total absorbed power by the plasma is $P = 20.41$ MW.) Figure 4(a) shows the density profile and temperature profiles are demonstrated in Fig.4(b). When compared to the ECW heating only case (Fig.3) the ion temperature is close to that of electrons. We obtain $< n_e > \simeq \bar{n}_e \simeq 1.0 \times 10^{20}$ m^{-3}, $T_{e0} = 2.72$ keV, $< T_e >= 1.36$ keV, $T_{i0} = 2.60$ keV, $< T_i >= 1.33$ keV, and $\tau_E^G = 98$ ms. The energy confinement times defined by the heat flux across the outermost flux surface are, $\tau_{Ee}^T = 84$ ms, $\tau_{Ei}^T = 186$ ms, and $\tau_E^T = 115$ ms. The anomalous electron heat flux dominates at the peripheral region as in the ECW case. The collisionalities for electrons and ions and the electric potential are shown in Fig.4(c) and (d), respectively.

4. Toroidal currents

The remarkable feature of neoclassical bootstrap current in stellarators/torsatrons is its strong dependence on the magnetic field configuration. The magnitudes and profiles of bootstrap currents in the LHD with $R = 5$ m have been examined by Nakajima et al.[22], in which it was revealed that shifting of the plasma in terms of the dipole field control is effective and the elipticity of magnetic surfaces, which can be controlled by the quadrupole field, have a remarkable influence on the bootstrap current : a small outward shift of the plasma and vertically elongated magneitc surfaces are favourable for a reduction of the bootstrap current. The bootstrap current depends on the pitch modulation α, but its dependence is not so strong. Figure 5 shows the dependence of bootstrap currents on α for the case of $B = 4$ T, $R = 4$ m, $a = 0.52$ m, $\gamma_c = 1.20$, and $\Delta_{axis} = -0.1$ m and $B_Q(net) \simeq 0$

(which is a little different parameter set from the proposed standard configuration described in §2). We have used the equations for bootstrap current in the $1/\nu$ regime given by Shaing and Callen [23]. In Fig.5, the rotational transform of the vacuum magnetic field ι_V and the total rotational transform ι_t, which consists of ι_V and that produced by the bootstrap current, are shown by the broken and solid curves, respectively. We see that the bootstrap current I_{bs} is larger for $\alpha < 0$ than for $\alpha > 0$ (it should be noted that $\alpha < 0$ is favorable for the single particle confinement) but the dependence on α is not so strong. For $\alpha = 0.1$ we have $I_{bs} \simeq 150$ kA and $(\Delta\iota)_{max} \simeq 10\%$, where $\Delta\iota = |(\iota_t - \iota_V)/\iota_V|$.

The proposed standard configuration for the LHD has been chosen so as to satisfy a good single particle confinement and a high β value. It is necessary to estimate the bootstrap current and beam driven current in this configuration. We consider these toroidal currents for the plasma heated by NBI (Fig.4). As is seen from Fig.4(c) the LHD plasma lies in the $1/\nu$ regime in the region of $r = 0.2 \sim 0.6$ m. We calculate the geometric factor given by Shaing and Callen [23] for the standard configuration assuming that the plasma is in the $1/\nu$ regime in the whole region. We use the profiles for $n_e(r)$, $T_e(r)$ and $T_i(r)$ obtained in Figs.4(a) and (b). The bootstrap current in the standard vacuum magnetic field amounts to $I_{bs} \simeq 169$ kA for the predicted plasma profiles.

Nakajima and Okamoto [24] have studied the neoclassical expression for the beam driven (or Ohkawa) current based on the drift kinetic equation for electrons in the $1/\nu$ regime. The net beam driven current density J_{net} is the sum of the fast ion beam current density J_b and the electron current density $J_{\|e}$ produced by the interactions with fast ions : $J_{net} = J_b + J_{\|e}$. In Ref.[24], $J_{\|e}$, or $F(= J_{net}/J_b)$, and the electric conductivity σ are derived for nonaxisymmetric devices. It is found that the strong configuration dependences are not seen for F and σ contrary to the bootstrap current since the interactions between electrons and fast ions or the inductive field occur in the velocity space. The different trapped electron distributions produce different beam currents and conductivities between the axisymmetric and nonaxisymmetric systems.

We estimate the beam driven current in the LHD plsama produced by the tangential neutral beam injections. Two neutral beams are injected in the same direction from the negative ion sources with the energy of 125 keV and the power of 10 MW. It is necessary to

calculate the fast ion beam current J_b to obtain the net beam driven current. In order to calculate J_b we solve the Fokker-Planck equations for fast ions with $v_{thi} \ll v_b \ll v_{the}$ [25], where v_{thi} and v_{the} are the plasma ion and electron thermal speeds, respectively, and v_b the beam ion speed. We assume that all the fast ions have the same speed v_b^0 and the same pitch angle θ_b^0 when they are generated by the injection of neutral atoms. Accordingly the source function for the fast ions is expressed by $S = S_0\delta(v - v_b^0)\delta(\cos\theta - \cos\theta_b^0)/v^2$. For this source function the Fokker-Planck equation has the steady state solution [25] and the beam current density is given by

$$J_b = Z_b e S_0 \tau_s \cos\theta_b^0 v_b^0 \frac{1}{1+\alpha^3} \int_0^1 \mathrm{d}x \cdot x^{3+Z_2} \left(\frac{1+\alpha^3}{x^3+\alpha^3}\right)^{1+Z_2/3} \tag{4.1}$$

where $S_0 = I_b/eZ_b$ with I_b the equivalent current and Z_b the beam atomic charge number, τ_s the slowing down time, $Z_2 = Z_{eff}/Z_1$ ($Z_1 = \sum_i n_i Z_i^2 m_b/n_e m_i$), and $\alpha = v_c/v_b^0$ (v_c is the critical speed [25]).

We calculate the beam driven current for the standard configuration of the LHD and the profiles of density and temperatures obtained in Fig.4(a) and (b). For simplicity we assume that the birth distribution of fast ions with 125 keV energy is a Gaussian profile centered at $r = 0$ and its halfwidth is $\Delta = a/4$. Z_{eff} is constant with the radius and $Z_2 = 1$ for the hydrogen beam atoms and hydrogen plasma ions. In Figs.6(a), (b), (c), and (d), the trapped electron distribution f_t, the function F, the beam current J_b, and the net beam driven currents J_{net} are shown, respectively. The fraction of trapped particles increases with the radius since the helical ripples increase with the radius. Accordingly the conductivity decreases with the radius although it is not shown in Figures. The function F, which reflects the effect of the elctron return current, inreases with the radius as the trapped particle fraction f_t increases and thereby the electron return current $J_{\|e}$ decreases. This is because of the fact that the number of passing electrons carrying the return current decreases with the increase in trapped electrons and that the passing electrons suffer from the frictional force against the trapped electrons. F also increases as the effective ionic charge number Z_{eff}. The radial dependences of F are weakened as Z_{eff} increases. For small Z_{eff} ($Z_{eff} \simeq 1.0$), the effect of f_t is singnificant, and the radial dependence of F is roughly the same as that of f_t. For large Z_{eff} ($Z_{eff} \geq 3$) f_t is less effective and F is a weak function of the radius. These results are attributed to the fact that increasing Z_{eff}

enhances the pitch angle scattering resulting in decrease in the electron return current. In the present case since Z_{eff} is constant $J_{\|e}$ is reduced uniformly and F approaces unity. In Fig.6(c) the beam currents calculated from Eq.(4.1) are shown. The profiles are assumed to be Gaussian but the magnitude of the beam current depends strongly on Z_{eff}. In Fig.6(d), the profiles of the net beam driven currents are shown. F increases with Z_{eff} whereas J_b decreases with Z_{eff} and the dependence of J_{net} on Z_{eff} is determined by the balance between the two different dependences. The total net beam current I_b can be obtained by the integration of J_{net} over the radius. For $Z_{eff} = 1 \sim 5$, the total currents amount to $I_b = 115 \sim 275$ kA when the beam power is 10 MW.

5. Conclusion

In this report we obtained the pofiles of density, temperatures and electric field in the LHD plasma by the transport code using the modified GRB scaling for the anomalous transport coefficients. The GRB scaling is used as the volume-averaged value of the anomalous coefficient but the radial profile of the coefficient, which has larger values in the edge region, has been given so as to reproduce the LHD scaling.

Using the density and temperature profiles obtained by the transport code we calculated the bootstrap current in the LHD plasma with the set of standard machine parameters given in §2. The bootstrap current amounts to $I_{bs} \simeq 169$ kA for the standard vacuum field configuration of the LHD and for the plasma profiles given in Fig.4. The estimated beam-driven current in the LHD plasma produced by the tangential neutral beam injection changes from 115 to 275 kA depending on Z_{eff} for the hydrogen neutral beams with energy of 125 keV and power of 10 MW. The bootstrap current and the beam driven current have been estimated only for the case of $\langle n_e \rangle \simeq \bar{n}_e \simeq 1 \times 10^{20} \mathrm{m}^{-3}$. The bootstrap current as well as the beam driven current can be easily influenced by various plasma profiles. Therefore it should be noted that the predicted values of the bootstrap current and beam driven current presented here are just the results only for the profiles given in Fig.4. Since the global confinement is governed dominantly by the anomalous transport coefficients, a model of the anomalous transport, which is derived from the reliable theory and describes accurately both the global confinement time scaling and the local dependence of the transport coeffi-

cients, is required. We have used the vacuum magnetic field configuration for calculations of bootstrap current and beam-driven current. It is well known that the bootstrap current depends strongly on the field configuration or the Fourier spectra of the magnetic fields, which can be modified by the finite beta effects. In order to obtain the more accurate results, it is necessary to solve three-dimensional equilibria with finite β including self-consistently the bootstrap current and beam-driven current. It is noticed that the parallel viscosities due to impuity ions and fast ions are important for the estimation of bootstrap current [26]. These problems are under investigation.

Acknowledgement

The authors are grateful to Dr. Y. Nakamura and Prof. M. Wakatani for providing the transport code and fruitful discussions. This work was partly supported by the Grant-in-Aid program from the Ministry of Education, Science and Culture.

References

[1] S. Sudo, Y. Takeiri, H. Zushi, F. Sano, K. Itoh, K. Kondo and A. Iiyoshi : Nucl. Fusion **30** (1990) 11.

[2] M. Murakami et al. : 13th Intern. Cof. on Plasma Phys. Contr. Nucl. Fus. Res., Washington, Oct., 1990, IAEA-CN-53/C-1-3.

[3] O. Kaneko et al. : 13th Intern. Cof. on Plasma Phys. Contr. Nucl. Fus. Res., Washington, Oct., 1990, IAEA-CN-53/C-1-4.

[4] S. Sudo : *"Global Confinement of Helical Systems"*, Workshop on the Large Helical Device, National Institute for Fusion Science, Nagoya, 8 Feb. 1990.

[5] H. Renner et al. : 13th Intern. Cof. on Plasma Phys. Contr. Nucl. Fus. Res., Washington, Oct., 1990, IAEA-CN-53/C-1-2.

[6] Design Report of the Large Helical Device I : Research Report of National Institute for Fusion Science, NIFS LHD Tech. Rep. **1**, June 1990 (in Japanese).

[7] K. Yamazaki and LHD Design Group : *"LHD Physics Design"*, IAEA Stellarator Workshop on Future Large Devices, Fusion Engineering Design Center, Oak Ridge, Tenessee, USA, Oct. 8–10, 1990, Vol.1.

[8] J. Todoroki : J. Phys. Soc. Jpn. **59** (1990) 2758.

[9] R. Goldston et al. : Bull. Am. Phys. Soc. **34** (1989) 1964.

[10] P. C. Liewer : Nucl. Fusion **25** (1985) 543.

[11] F. Sano et al. : *"Parametric Scaling Studies of Energy-Confinement Time for Neutral-Beam-Heated Helotron E Plasmas"*, Res. Rep. of Plasma Phys. Lab., Kyoto Univ., **PPLK-R-38**, Feb. 1989.

[12] M. Okamoto et al. : Jpn. J. Appl. Phys. **22** (1983) L686.

[13] W. K. Hagan and E. A. Frieman : Phys. Fluids **29** (1986) 3635.

[14] J. W. Connor : Plasma Phys. Controll. Fusion **30** (1988) 619.

[15] E. A. Frieman and L. Chen : Phys. Fluids **25** (1982) 502.

[16] J. P. Christiansen et al. : Nucl. Fusion **30** (1990) 1183.

[17] Y. Nakamura and M. Wakatani : *"Transport Simulations of New Stellarator/Helotron Devices Based on the Neoclassical Ripple Transport with an Edge Turbulence"*, Res. Rep. of Plasma Phys. Lab., Kyoto Univ., **PPLK-R-24**, Feb. 1989.

[18] K. C. Shaing, Y. Nakamura and M. Wakatani : Phys. Fluids **31** (1988) 1288.

[19] D. E. Hasting, W. A. Houlberg, and K. C. Shaing : Nucl. Fusion **25**(1985)445.

[20] N. Nakajima, T. Amano and M. Okamoto : in preparation for publication.

[21] Y. Ogawa, T. Amano, N. Nakajima, Y. Ohyabu, K. Yamazaki, S. P. Hirshman, W. I. van Rij, and K. C. Shaing : to appear in Research Report of National Institute for Fusion Science, NIFS Rep., September 1991.

[22] N. Nakajima, M. Okamoto, J. Todoroki, Y. Nakamura and M. Wakatani : Nucl. Fusion **29** (1989) 605.

[23] K. C. Shaing and J. D. Callen : Nucl. Fusion **26** (1983) 3315.

[24] N. Nakajima and M. Okamoto : J Phys. Soc. Jpn. **59** (1990) 3595.

[25] J. D. Gaffey Jr. : J. Plasma Phys. **16**, part 2 (1976) 149.

[26] M. Kikuchi, M. Azumi, S. Tsuji, K. Tani and H. Kubo : Nucl. Fusion **30** (1990) 343.

Figure captions

Fig.1 Diagram of LHD empirical scaling law. τ_E[s], β[%], T[keV] and $n_e[10^{20}\mathrm{m}^{-3}]$ are shown for $B = 4$ T, $R = 3.9$ m and $a = 0.65$ m.

Fig.2 Comparison of LHD empirical scaling law and transpot code results.

Fig.3 Transport code results in the case of ECW heating. $B = 4$ T, $R = 3.9$ m, $a = 0.6$ m.

(a) density profile, (b) temperature profiles for electrons (solid line) and ions (dashed line). (c) electron thermal diffusivities : ripple diffusion (dot-dashed line) axisymmetric neoclassical diffusion (dashed line), anomalous diffusion (2 dots-dashed line), total coefficient (solid line). (d) ion thermal diffusivities : ripple diffusion (dot-dashed line) axisymmetric neoclassical diffusion (dashed line), total coefficient (solid line), anomalous diffusion is not included. (e) collisionalities for electrons ν_{e**} (solid line) and ions ν_{i**} (dashed line). (f) electric potential calculated from $\Gamma_e(E_r) = \Gamma_i(E_r)$.

Fig.4 Transport code results in the case of NBI heating. Hydrogen neutral beams with energy of 125 keV and power of 20 MW are injected tangentially to the hydrogen plasma. ECW heating with 3 MW is added. Other parameters are the same as in Fig.3.

(a) density profile, (b) electron and ion temperature profiles, (c) collisionalities for electrons and ions, (d) electric potential profile.

Fig.5 Bootatrap current dependence on the pitch modulation parameter α. The geometric factor is calculated for the vacuum field with $B = 4$ T, $R = 4$ m, $a = 0.52$ m, $\gamma_c = 1.20$, $\Delta_{axis} = -0.1$ m and $B_Q(net) \simeq 0$ (a little different from the standard configuration). Plasma profiles are calculated by the transport code for $B = 4$ T, $R = 4$ m and $a = 0.52$ m (different from the results in Figs.3 and 4).

Fig.6 Beam driven current. The beam power is 10 MW and other beam parameters are the same as in Fig.4.

(a) f_t : fraction of trapped electrons. (b) $F = J_{net}/J_b$. (c) J_b : beam current density, (d) J_{net} : net beam current density.

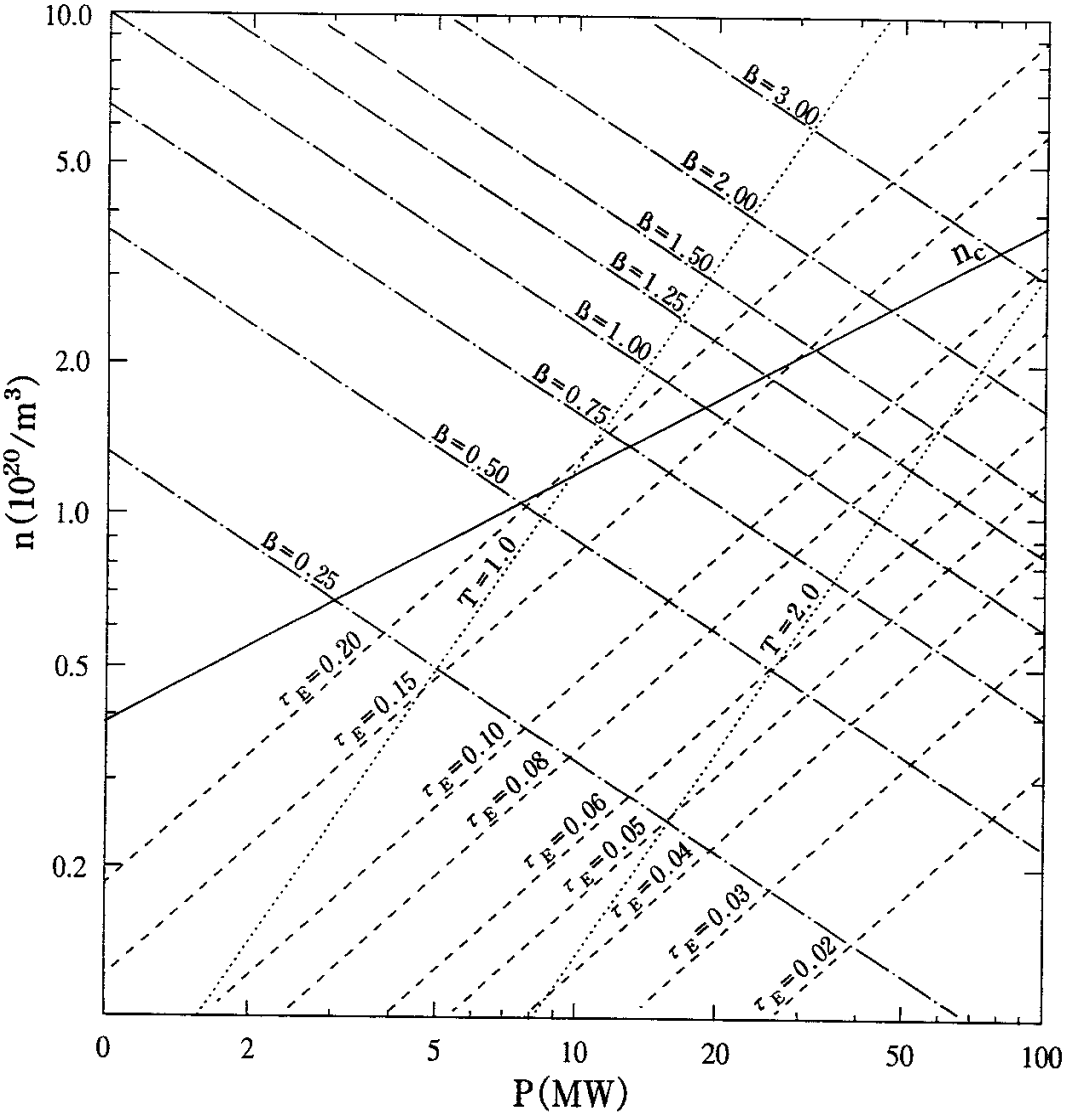
10.0
5.0
2.0
1.0
0.5
0.2
n(10^20/m^3)
0
2
5
10
20
50
100
P(MW)
β=3.00
β=2.00
β=1.50
β=1.25
β=1.00
β=0.75
β=0.50
β=0.25
nc
T=1.0
T=2.0
τE=0.20
τE=0.15
τE=0.10
τE=0.08
τE=0.06
τE=0.05
τE=0.04
τE=0.03
τE=0.02

Fig. 1

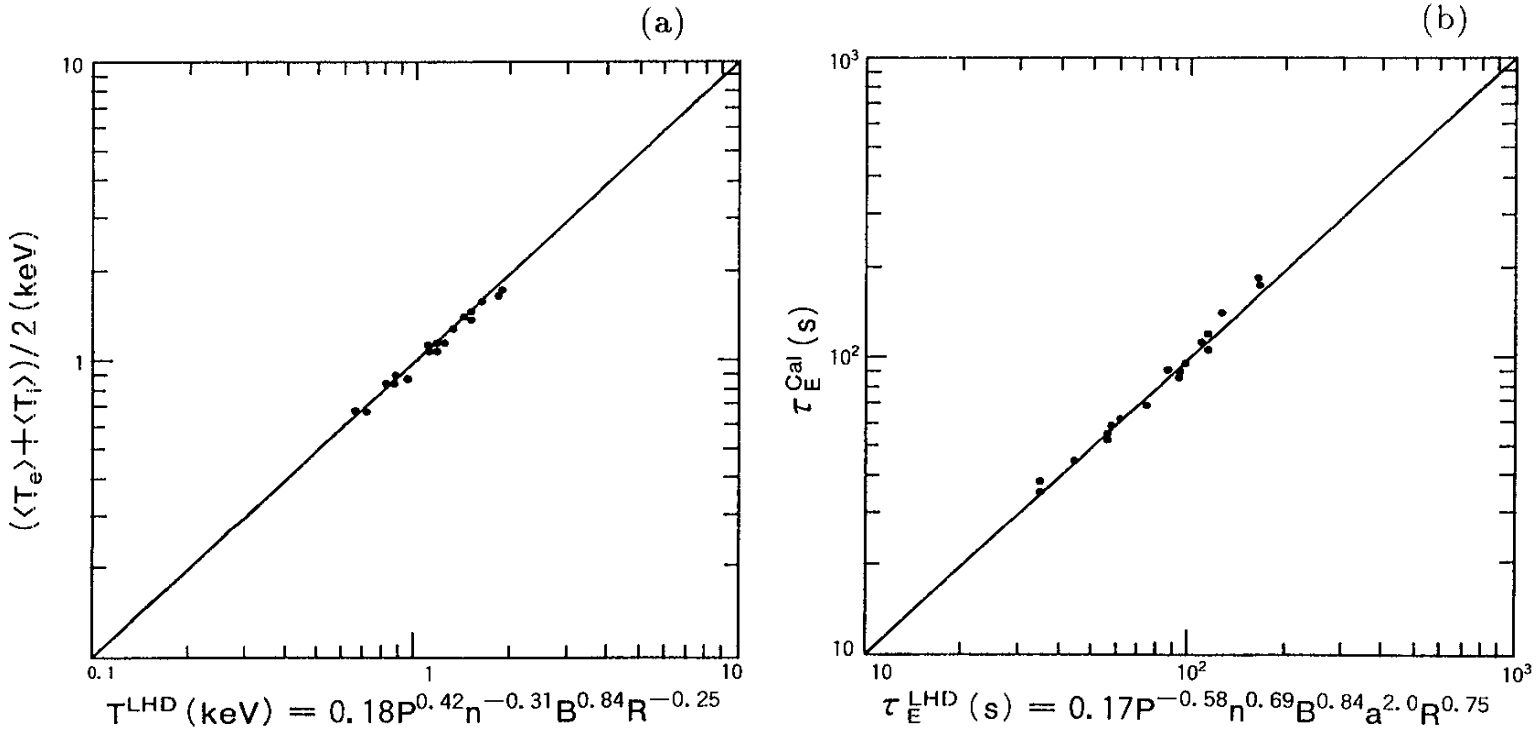
(a)
10
1
0.1
1
10
$(\langle T_e\rangle+\langle T_i\rangle)/2$ (keV)
T^{LHD} (keV) $= 0.18P^{0.42}n^{-0.31}B^{0.84}R^{-0.25}$
(b)
10^3
10^2
10
τ_E^{Cal} (s)
10
10^2
10^3
τ_E^{LHD} (s) $= 0.17P^{-0.58}n^{0.69}B^{0.84}a^{2.0}R^{0.75}$

Fig.2

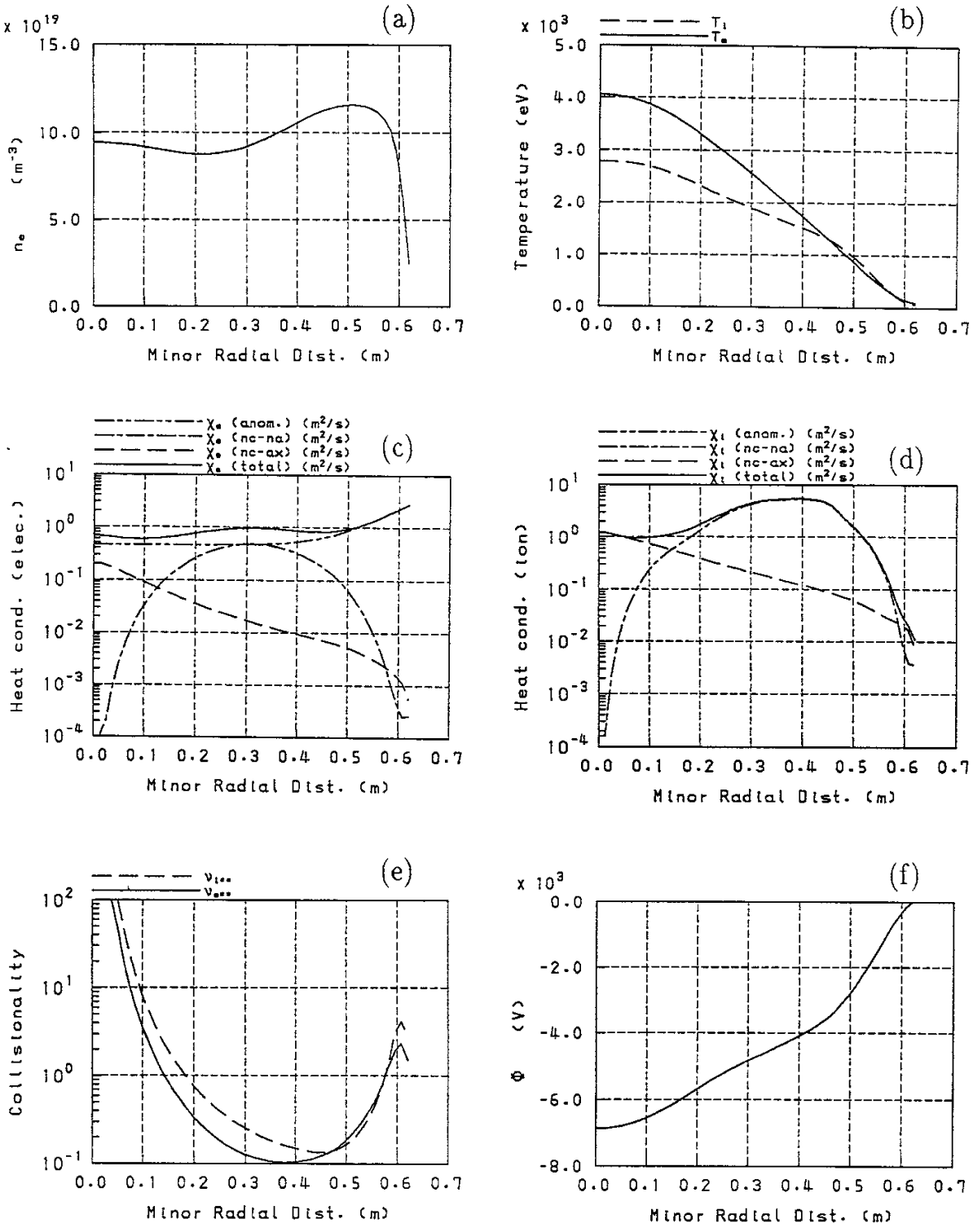
(a)
x 10^19
15.0
10.0
5.0
0.0
n_e (m^-3)
0.0 0.1 0.2 0.3 0.4 0.5 0.6 0.7
Minor Radial Dist. (m)
(b)
x 10^3
T_i
T_e
5.0
4.0
3.0
2.0
1.0
0.0
Temperature (eV)
0.0 0.1 0.2 0.3 0.4 0.5 0.6 0.7
Minor Radial Dist. (m)
(c)
χ_e (anom.) (m^2/s)
χ_e (nc-na) (m^2/s)
χ_e (nc-ax) (m^2/s)
χ_e (total) (m^2/s)
10^1
10^0
10^-1
10^-2
10^-3
10^-4
Heat cond. (elec.)
0.0 0.1 0.2 0.3 0.4 0.5 0.6 0.7
Minor Radial Dist. (m)
(d)
χ_i (anom.) (m^2/s)
χ_i (nc-na) (m^2/s)
χ_i (nc-ax) (m^2/s)
χ_i (total) (m^2/s)
10^1
10^0
10^-1
10^-2
10^-3
10^-4
Heat cond. (ion)
0.0 0.1 0.2 0.3 0.4 0.5 0.6 0.7
Minor Radial Dist. (m)
(e)
ν_i**
ν_e**
10^2
10^1
10^0
10^-1
Collisionality
0.0 0.1 0.2 0.3 0.4 0.5 0.6 0.7
Minor Radial Dist. (m)
(f)
x 10^3
0.0
-2.0
-4.0
-6.0
-8.0
Φ (V)
0.0 0.1 0.2 0.3 0.4 0.5 0.6 0.7
Minor Radial Dist. (m)

Fig.3

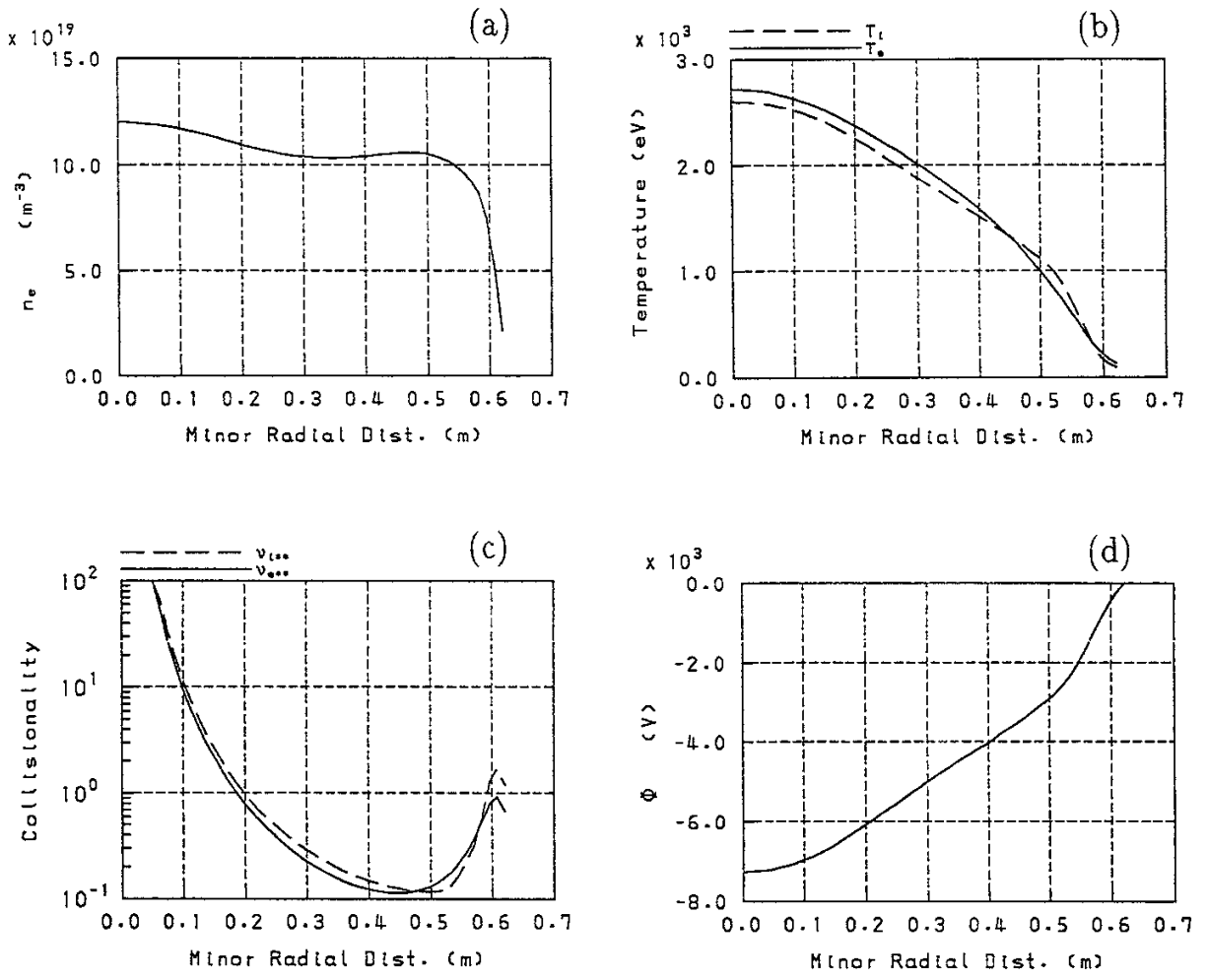
(a)
x 10^19
15.0
10.0
5.0
0.0
n_e (m^-3)
0.0 0.1 0.2 0.3 0.4 0.5 0.6 0.7
Minor Radial Dist. (m)
(b)
x 10^3
T_i
T_e
3.0
2.0
1.0
0.0
Temperature (eV)
0.0 0.1 0.2 0.3 0.4 0.5 0.6 0.7
Minor Radial Dist. (m)
(c)
ν_i**
ν_e**
10^2
10^1
10^0
10^-1
Collisionality
0.0 0.1 0.2 0.3 0.4 0.5 0.6 0.7
Minor Radial Dist. (m)
(d)
x 10^3
0.0
-2.0
-4.0
-6.0
-8.0
Φ (V)
0.0 0.1 0.2 0.3 0.4 0.5 0.6 0.7
Minor Radial Dist. (m)

Fig.4

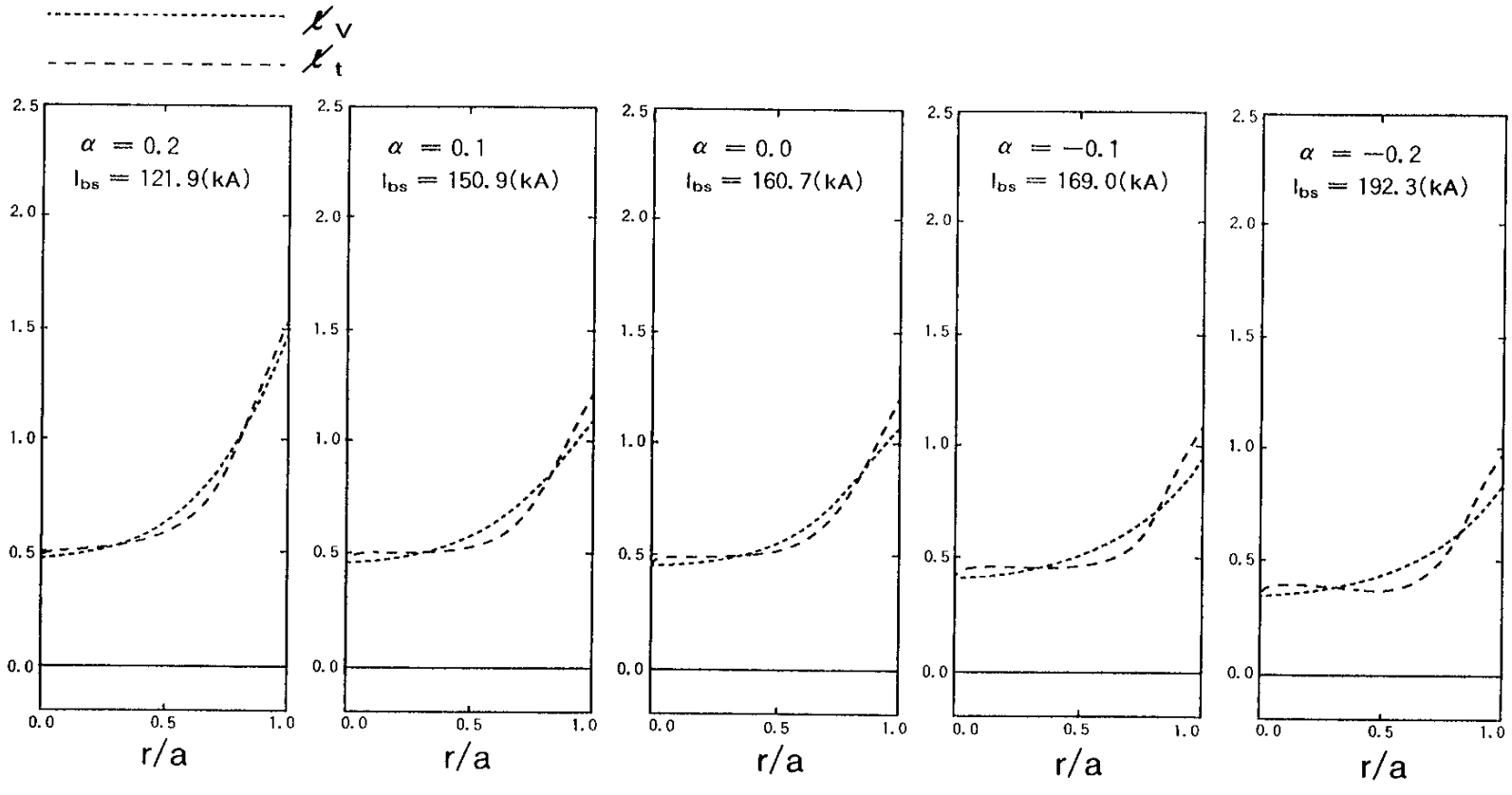
ι_V
ι_t
α = 0.2
I_{bs} = 121.9(kA)
α = 0.1
I_{bs} = 150.9(kA)
α = 0.0
I_{bs} = 160.7(kA)
α = −0.1
I_{bs} = 169.0(kA)
α = −0.2
I_{bs} = 192.3(kA)
2.5
2.0
1.5
1.0
0.5
0.0
0.0
0.5
1.0
r/a

Fig.5

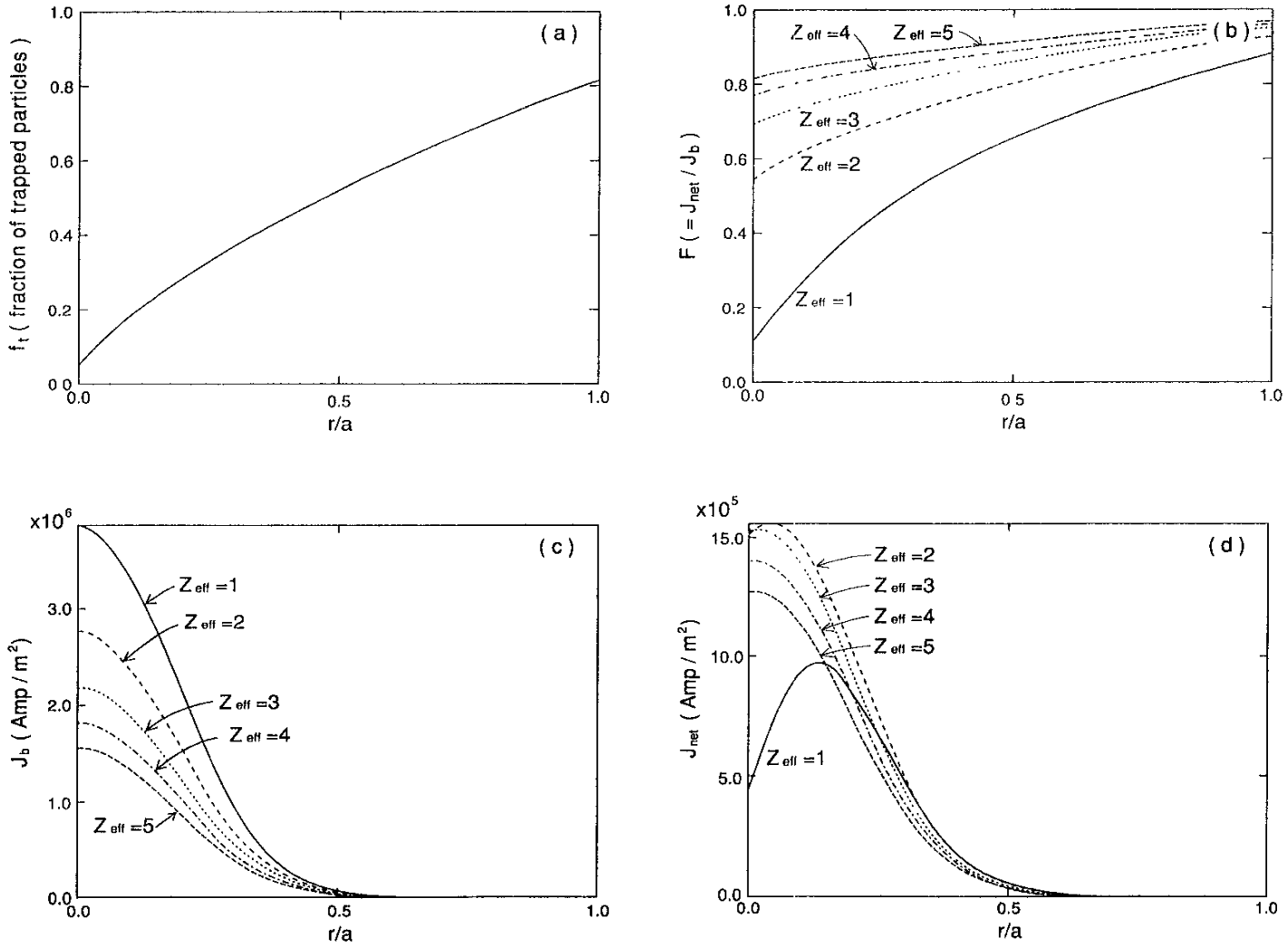
(a)
f_t (fraction of trapped particles)
r/a
(b)
F (= J_{net} / J_b)
Z_{eff} =4
Z_{eff} =5
Z_{eff} =3
Z_{eff} =2
Z_{eff} =1
r/a
(c)
x10^6
J_b (Amp / m^2)
Z_{eff} =1
Z_{eff} =2
Z_{eff} =3
Z_{eff} =4
Z_{eff} =5
r/a
(d)
x10^5
J_{net} (Amp / m^2)
Z_{eff} =2
Z_{eff} =3
Z_{eff} =4
Z_{eff} =5
Z_{eff} =1
r/a

Fig.6

Recent Issues of NIFS Series

NIFS-53 M.Okamoto and N.Nakajima, *Bootstrap Currents in Stellarators and Tokamaks*; Sep. 1990

NIFS-54 K.Itoh and S.-I.Itoh, *Peaked-Density Profile Mode and Improved Confinement in Helical Systems*; Oct. 1990

NIFS-55 Y.Ueda, T.Enomoto and H.B.Stewart, *Chaotic Transients and Fractal Structures Governing Coupled Swing Dynamics*; Oct. 1990

NIFS-56 H.B.Stewart and Y.Ueda, *Catastrophes with Indeterminate Outcome*; Oct. 1990

NIFS-57 S.-I.Itoh, H.Maeda and Y.Miura, *Improved Modes and the Evaluation of Confinement Improvement*; Oct. 1990

NIFS-58 H.Maeda and S.-I.Itoh, *The Significance of Medium- or Small-size Devices in Fusion Research*; Oct. 1990

NIFS-59 A.Fukuyama, S.-I.Itoh, K.Itoh, K.Hamamatsu, V.S.Chan, S.C.Chiu, R.L.Miller and T.Ohkawa, *Nonresonant Current Drive by RF Helicity Injection*; Oct. 1990

NIFS-60 K.Ida, H.Yamada, H.Iguchi, S.Hidekuma, H.Sanuki, K.Yamazaki and CHS Group, *Electric Field Profile of CHS Heliotron/Torsatron Plasma with Tangential Neutral Beam Injection*; Oct. 1990

NIFS-61 T.Yabe and H.Hoshino, *Two- and Three-Dimensional Behavior of Rayleigh-Taylor and Kelvin-Helmholz Instabilities*; Oct. 1990

NIFS-62 H.B. Stewart, *Application of Fixed Point Theory to Chaotic Attractors of Forced Oscillators;* Nov. 1990

NIFS-63 K.Konn., M.Mituhashi, Yoshi H.Ichikawa,*Soliton on Thin Vortex Filament;* Dec. 1990

NIFS-64 K.Itoh, S.-I.Itoh and A.Fukuyama,*Impact of Improved Confinement on Fusion Research;* Dec. 1990

NIFS -65 A.Fukuyama, S.-I.Itoh and K. Itoh,*A Consistency Analysis on the Tokamak Reactor Plasmas;* Dec. 1990

NIFS-66 K.Itoh, H. Sanuki, S.-I. Itoh and K. Tani,*Effect of Radial Electric Field on α-Particle Loss in Tokamaks;* Dec. 1990

NIFS-67 K.Sato,and F.Miyawaki,*Effects of a Nonuniform Open Magnetic Field on the Plasma Presheath*; Jan.1991

NIFS-68 K.Itoh and S.-I.Itoh,*On Relation between Local Transport Coefficient and Global Confinement Scaling Law;* Jan. 1991

NIFS-69 T.Kato, K.Masai, T.Fujimoto,F.Koike, E.Källne, E.S.Marmar and J.E.Rice,*He-like Spectra Through Charge Exchange Processes in Tokamak Plasmas;* Jan.1991

NIFS-70 K. Ida, H. Yamada, H. Iguchi, K. Itoh and CHS Group, *Observation of Parallel Viscosity in the CHS Heliotron/Torsatron* ; Jan.1991

NIFS-71 H. Kaneko, *Spectral Analysis of the Heliotron Field with the Toroidal Harmonic Function in a Study of the Structure of Built-in Divertor* ; Jan. 1991

NIFS-72 S. -I. Itoh, H. Sanuki and K. Itoh, *Effect of Electric Field Inhomogeneities on Drift Wave Instabilities and Anomalous Transport* ; Jan. 1991

NIFS-73 Y.Nomura, Yoshi.H.Ichikawa and W.Horton, *Stabilities of Regular Motion in the Relativistic Standard Map*; Feb. 1991

NIFS-74 T.Yamagishi, *Electrostatic Drift Mode in Toroidal Plasma with Minority Energetic Particles*, Feb. 1991

NIFS-75 T.Yamagishi, *Effect of Energetic Particle Distribution on Bounce Resonance Excitation of the Ideal Ballooning Mode*, Feb. 1991

NIFS-76 T.Hayashi, A.Tadei, N.Ohyabu and T.Sato, *Suppression of Magnetic Surface Breading by Simple Extra Coils in Finite Beta Equilibrium of Helical System;* Feb. 1991

NIFS-77 N. Ohyabu, *High Temperature Divertor Plasma Operation*; Feb. 1991

NIFS-78 K.Kusano, T. Tamano and T. Sato, *Simulation Study of Toroidal Phase-Locking Mechanism in Reversed-Field Pinch Plasma*; Feb. 1991

NIFS-79 K. Nagasaki, K. Itoh and S. -I. Itoh, *Model of Divertor Biasing and Control of Scrape-off Layer and Divertor Plasmas*; Feb. 1991

NIFS-80 K. Nagasaki and K. Itoh, *Decay Process of a Magnetic Island by Forced Reconnection*; Mar. 1991

NIFS-81 K. Takahata, N. Yanagi, T. Mito, J. Yamamoto, O.Motojima and LHDDesign Group, K. Nakamoto, S. Mizukami, K. Kitamura, Y. Wachi, H. Shinohara, K. Yamamoto, M. Shibui, T. Uchida and K. Nakayama, *Design and Fabrication of Forced-Flow Coils as R&D Program for Large Helical Device*; Mar. 1991

NIFS-82 T. Aoki and T. Yabe, *Multi-dimensional Cubic Interpolation for ICF Hydrodynamics Simulation*; Apr. 1991

NIFS-83 K. Ida, S.-I. Itoh, K. Itoh, S. Hidekuma, Y. Miura, H. Kawashima, M. Mori, T. Matsuda, N. Suzuki, H. Tamai, T.Yamauchi and JFT-2M Group, *Density Peaking in the JFT-2M Tokamak Plasma with Counter Neutral Beam Injection* ; May 1991

NIFS-84 A. Iiyoshi, *Development of the Stellarator/Heliotron Research*; May 1991

NIFS-85 Y. Okabe, M. Sasao, H. Yamaoka, M. Wada and J. Fujita, *Dependence of Au^- Production upon the Target Work Function in a Plasma-Sputter-Type Negative Ion Source;* May 1991

NIFS-86 N. Nakajima and M. Okamoto, *Geometrical Effects of the Magnetic Field on the Neoclassical Flow, Current and Rotation in General Toroidal Systems*; May 1991

NIFS-87 S. -I. Itoh, K. Itoh, A. Fukuyama, Y. Miura and JFT-2M Group, *ELMy-H mode as Limit Cycle and Chaotic Oscillations in Tokamak Plasmas;* May 1991

NIFS-88 N.Matsunami and K.Kitoh, *High Resolution Spectroscopy of H^+ Energy Loss in Thin Carbon Film;* May 1991

NIFS-89 H. Sugama, N. Nakajima and M.Wakatani, *Nonlinear Behavior of Multiple-Helicity Resistive Interchange Modes near Marginally Stable States;* May 1991

NIFS-90 H. Hojo and T.Hatori, *Radial Transport Induced by Rotating RF Fields and Breakdown of Intrinsic Ambipolarity in a Magnetic Mirror*; May 1991

NIFS-91 M. Tanaka, S. Murakami, H. Takamaru and T.Sato, *Macroscale Implicit, Electromagnetic Particle Simulation of Inhomogeneous and Magnetized Plasmas in Multi-Dimensions;* May 1991

NIFS-92 S. - I. Itoh, *H-mode Physics, -Experimental Observations and Model Theories-, Lecture Notes, Spring College on Plasma Physics, May 27 - June 21 1991 at International Centre for Theoretical Physics (IAEA UNESCO) Trieste, Italy ;* Jun. 1991

NIFS-93 Y. Miura, K. Itoh, S. - I. Itoh, T. Takizuka, H. Tamai, T. Matsuda, N. Suzuki, M. Mori, H. Maeda and O. Kardaun, *Geometric Dependence of the Scaling Law on the Energy Confinement Time in H-mode Discharges;* Jun. 1991

NIFS-94 H. Sanuki, K. Itoh, K. Ida and S. - I. Itoh, *On Radial Electric Field Structure in CHS Torsatron / Heliotron;* Jun. 1991

NIFS-95 K. Itoh, H. Sanuki and S. - I. Itoh, *Influence of Fast Ion Loss on Radial Electric Field in Wendelstein VII-A Stellarator;* Jun. 1991

NIFS-96 S. - I. Itoh, K. Itoh, A. Fukuyama, *ELMy-H mode as Limit Cycle and Chaotic Oscillations in Tokamak Plasmas;* Jun. 1991

NIFS-97 K. Itoh, S. - I. Itoh, H. Sanuki, A. Fukuyama, *An H-mode-Like Bifurcation in Core Plasma of Stellarators;* Jun. 1991

NIFS-98 H. Hojo, T. Watanabe, M. Inutake, M. Ichimura and S. Miyoshi, *Axial Pressure Profile Effects on Flute Interchange Stability in the Tandem Mirror GAMMA 10;* Jun. 1991

NIFS-99 A. Usadi, A. Kageyama, K. Watanabe and T. Sato, *A Global Simulation of the Magnetosphere with a Long Tail : Southward and Northward IMF;* Jun. 1991

NIFS-100 H. Hojo, T. Ogawa and M. Kono, *Fluid Description of Ponderomotive Force Compatible with the Kinetic One in a Warm Plasma* ; July 1991

NIFS-101 H. Momota, A. Ishida, Y. Kohzaki, G. H. Miley, S. Ohi, M. Ohnishi K. Yoshikawa, K. Sato, L. C. Steinhauer, Y. Tomita and M. Tuszewski *Conceptual Design of D-^{3}He FRC Reactor "ARTEMIS"* ; July 1991

NIFS-102 N. Nakajima and M. Okamoto, *Rotations of Bulk Ions and Impurities in Non-Axisymmetric Toroidal Systems* ; July 1991

NIFS-103 A. J. Lichtenberg, K. Itoh, S. - I. Itoh and A. Fukuyama, *The Role of Stochasticity in Sawtooth Oscillation* ; Aug. 1991

NIFS-104 K. Yamazaki and T. Amano, *Plasma Transport Simulation Modeling for Helical Confinement Systems;* Aug. 1991

NIFS-105 T. Sato, T. Hayashi, K. Watanabe, R. Horiuchi, M. Tanaka, N. Sawairi and K. Kusano, *Role of Compressibility on Driven Magnetic Reconnection ;* Aug. 1991

NIFS-106 Qian Wen - Jia, Duan Yun - Bo, Wang Rong - Long and H. Narumi, *Electron Impact Excitation of Positive Ions - Partial Wave Approach in Coulomb - Eikonal Approximation* ; Sep. 1991

NIFS-107 S. Murakami and T. Sato, *Macroscale Particle Simulation of Externally Driven Magnetic Reconnection;* Sep. 1991

NIFS-108 Y. Ogawa, T. Amano, N. Nakajima, Y. Ohyabu, K. Yamazaki, S. P. Hirshman, W. I. van Rij and K. C. Shaing, *Neoclassical Transport Analysis in the Banana Regime on Large Helical Device (LHD) with the DKES Code;* Sep. 1991

NIFS-109 Y. Kondoh, *Thought Analysis on Relaxation and General Principle to Find Relaxed State;* Sep. 1991

NIFS-110 H. Yamada, K. Ida, H. Iguchi, K. Hanatani, S. Morita, O. Kaneko, H. C. Howe, S. P. Hirshman, D. K. Lee, H. Arimoto, M. Hosokawa, H. Idei, S. Kubo, K. Matsuoka, K. Nishimura, S. Okamura, Y. Takeiri, Y. Takita and C. Takahashi, *Shafranov Shift in Low-Aspect-Ratio Heliotron / Torsatron CHS* ; Sep 1991

NIFS-111 R. Horiuchi, M. Uchida and T. Sato, *Simulation Study of Stepwise Relaxation in a Spheromak Plasma ;* Oct. 1991

NIFS-112 M. Sasao, Y. Okabe, A. Fujisawa, H. Iguchi, J. Fujita, H. Yamaoka and M. Wada, *Development of Negative Heavy Ion Sources for Plasma Potential Measurement* ; Oct. 1991

NIFS-113 S. Kawata and H. Nakashima, *Tritium Content of a DT Pellet in Inertial Confinement Fusion* ; Oct. 1991